

准三维功能梯度微梁的尺度效应模型 及微分求积有限元*

刘松正, 张波, 沈火明, 张旭

(西南交通大学 力学与工程学院, 成都 610031)

摘要: 基于修正的偶应力理论与四参数高阶剪切-法向伸缩变形理论, 提出了一种具有尺度依赖性的准三维功能梯度微梁模型, 并应用于小尺度功能梯度梁的静力弯曲和自由振动分析中. 采用第二类 Lagrange 方程, 推导了微梁的运动微分方程及边界条件. 针对一般边值问题, 构造了一种融合 Gauss-Lobatto 求积准则与微分求积准则的 2 节点 16 自由度微分求积有限元. 通过对比性研究, 验证了理论模型以及求解方法的有效性. 最后, 探究了梯度指数、内禀特征长度、几何参数及边界条件对微梁静态响应与振动特性的影响. 结果表明, 该文所发展的梁模型及微分求积有限元适用于研究各种长细比的功能梯度微梁的静/动力学问题, 引入尺度效应会显著地改变微梁的力学特性.

关键词: 修正的偶应力理论; 四参数高阶剪切-法向伸缩变形理论; 准三维功能梯度微梁; 微分求积有限元

中图分类号: TB383; TB34 **文献标志码:** A **DOI:** 10.21656/1000-0887.4100260

A Size-Dependent Quasi-3D Functionally Graded Microbeam Model and Related Differential Quadrature Finite Elements

LIU Songzheng, ZHANG Bo, SHEN Huoming, ZHANG Xu
(School of Mechanics & Engineering, Southwest Jiaotong University,
Chengdu 610031, P.R.China)

Abstract: A size-dependent quasi-3D functionally graded (FG) microbeam model was presented within the combined framework of the modified couple stress theory and a 4-unknown higher-order shear and normal deformation theory. Then the model was applied to analyze the static bending and free vibration of FG microbeams. With the 2nd Lagrange equation, the corresponding motion equations and the appropriate boundary conditions were obtained. A 2-node 16DOF differential quadrature finite element combining the Gauss-Lobatto quadrature rule with the differential quadrature rule was constructed to handle the general static/dynamic boundary value problems of FG microbeams. A comparison study was performed to show the efficacy of the proposed theoretical model and solution method. Finally, the effects of the gradient index, the intrinsic length

* 收稿日期: 2020-09-07; 修订日期: 2021-05-06

基金项目: 国家自然科学基金青年科学基金(11602204); 2020年度中央高校基本科研业务费基础研究培育项目(2682020ZT106)

作者简介: 刘松正(1995—), 男, 硕士生(E-mail: 635823637@qq.com);
张波(1984—), 男, 讲师, 博士(通讯作者. E-mail: zhangbo2008@home.swjtu.edu.cn).

引用格式: 刘松正, 张波, 沈火明, 张旭. 准三维功能梯度微梁的尺度效应模型及微分求积有限元[J]. 应用数学和力学, 2021, 42(6): 623-636.

scale parameter, the geometrical parameters and the boundary conditions on the static and dynamic characteristics of FG microbeams were examined. Numerical results reveal that the developed beam model and element are applicable to the analysis of mechanical behaviors of FG microbeams with various slenderness ratios. Besides, introduction of the couple stress effect can significantly change the static and dynamic characteristics of FG microbeams.

Key words: modified couple stress theory; 4-unknown higher-order shear and normal deformation theory; quasi-3D functionally graded microbeam; differential quadrature finite element

引 言

功能梯度材料是由两种或两种以上单相材料复合而成的多相材料,其物性参数沿特定方向呈连续梯度变化.因其利用连续变化的组分梯度来代替突变界面,从而有效地消除了层状结构中存在的应力集中和层间破坏等现象.随着微电子技术和超精密加工技术的发展,功能梯度材料的应用逐渐拓展至微/纳米机电系统领域.鉴于几何形状及受力特点,微/纳米机电系统中许多承载构件可以被简化为小尺度杆、梁、板、壳等.诸多实验已证实,微尺度结构的力学行为具有尺度效应^[1-3],原因在于小尺度构件的特征尺寸(如厚度、直径)与组分材料的内禀特征长度处于同一量级或者比较接近.经典连续介质力学由于具有尺度无关性,因而无法解释尺度效应.鉴于此,本构关系中包含材料内禀特征长度的非经典连续介质力学引起了研究者的兴趣.修正的应变梯度理论^[1]和修正的偶应力理论^[4]便是诸多非经典理论中的代表,前者引入了拉伸梯度张量、膨胀梯度张量、旋转梯度张量的对称部分,后者仅涉及旋转梯度张量的对称部分.由于修正的偶应力理论仅需要确定一个内禀特征长度,这为细观尺度梁、板结构的实验表征与理论分析带来了极大便利.

近年来,研究者将修正的偶应力理论与梁板结构的各种位移场假设相结合,开展了一系列关于微尺度复合材料结构的弯曲、振动、屈曲问题的研究工作^[5-13].Lei等^[7]基于修正的偶应力理论和 Reddy 型高阶剪切-法向伸缩变形理论,提出了一种五参数准三维功能梯度微板模型,并采用 Navier 法推导了四边简支情形下静力弯曲与自由振动的解析解.Nguyen等^[8]采用等几何分析方法,研究了任意形状准三维修正的偶应力功能梯度微板的静力弯曲、自由振动、屈曲问题.基于精化的锯齿理论和修正的偶应力理论,杨子豪等^[9]建立了一种能够有效预测功能梯度夹心微板挠度、位移、应力等静态响应的力学模型.曹源和雷剑^[12]提出了一种修正的偶应力正弦剪切变形板模型,然后将之应用于功能梯度三明治微梁的静态弯曲和自由振动分析中.Thai等^[13]推导了修正的偶应力准三维石墨烯增强功能梯度微板的运动微分方程和边界条件,采用等几何分析方法探讨了微板的自由振动和屈曲特性.

目前,有关修正的偶应力梁板结构力学问题的理论建模研究已经十分完善.然而,绝大多数微尺度梁板模型的建立是基于 Kirchhoff-Love 直线法假设、一阶剪切变形理论乃至高阶剪切变形理论,而垂直于结构中的面的法向伸缩变形效应往往被忽略.Carrera等^[14]指出考虑法向伸缩效应可以更加准确地预测复合材料厚梁或者厚板的静动力学响应.此后,研究者们发展了几种高阶剪切-法向伸缩变形理论来分析复合材料结构力学问题.Neves等^[15]建立了一种准三维双曲型高阶剪切-法向伸缩变形功能梯度板模型,借助于 Carrera 统一公式推导了板的运动方程和边界条件,利用径向基点插值无网格法求解了相应的边值问题.Lee等^[16]提出了一种包含五个位移场变量的修正的高阶剪切-法向变形板理论,据此分析了弹性地基上功能梯度板的力学行为.需要指出的是,将修正的偶应力理论与高阶剪切-法向伸缩变形理论相结合来研究微尺度功能梯度梁板结构力学问题的工作还比较少.此外,高阶位移梯度项的出现会导致微尺度结构力学模型控制方程的阶次显著升高和非经典边界条件的出现,位移场变量因此需要具备更高的连续性要求.鉴于标准有限元方法在实现位移场高阶连续性方面存在一定的局限性,Zhang等^[17-20]汲取微分求积法在实现位移场高阶连续性方面的优点以及有限元法在施加边界条件和对复杂求解域的强适应性等方面的优点,构造了一系列应变梯度/修正的偶应力梁板模型的微分求积有限元.

本文基于修正的偶应力理论与 Reddy 型四参数高阶剪切-法向伸缩变形理论,发展了一种准三维功能梯度微梁的尺度效应模型,运动方程和边界条件由第二类 Lagrange 方程导出.针对一般的边值问题,构造了一种 2 节点 16 自由度微分求积有限元.最后,比较了标准有限元与微分求积有限元的收敛性,分析了典型边界

条件下微梁的静力弯曲和振动问题,探究了内禀特征长度、长细比、梯度指数、法向伸缩效应及边界条件对微梁静动态特性的影响。

1 准三维功能梯度微梁的理论模型

1.1 准三维功能梯度微梁的等效材料参数

图 1 所示为一由陶瓷和金属组成的功能梯度微梁,其长度为 L , 宽度为 b , 高度为 h , 几何中面为 xOz 平面, 横向分布荷载为 q . 等效材料参数如弹性模量 E , 密度 ρ 和 Poisson 比 ν 被假定为沿高度方向连续地变化。

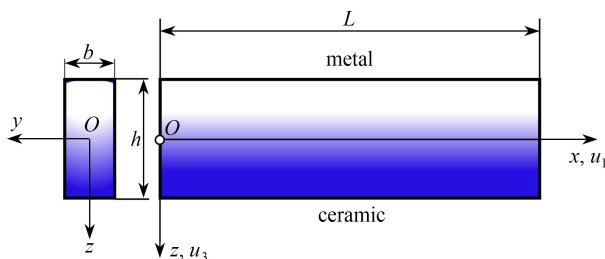


图 1 功能梯度微梁几何示意图

Fig. 1 Geometry schematic of an FG microbeam

基于 Voigt 线性混合律模型^[5], 功能梯度微梁的等效材料参数可以表示为

$$E(z) = E_m + (E_c - E_m) \cdot V_c(z), \rho(z) = \rho_m + (\rho_c - \rho_m) \cdot V_c(z), \nu(z) = \nu_m + (\nu_c - \nu_m) \cdot V_c, \quad (1)$$

式中 $V_c(z) = (1/2 + z/h)^n$ 表示陶瓷的体积分数, n 为梯度指数, 下角标 m 和 c 分别代表金属相和陶瓷相。

1.2 修正的偶应力理论

Yang 等^[4]通过在经典偶应力理论中引入新的力偶矩平衡方程, 将偶应力张量约束为对称形式, 由此发展出一种修正的偶应力理论. 在该理论框架下, 各向同性线弹性体的应变能 Π_s 为

$$\Pi_s = \int_{\Omega} (\sigma_{ij} \varepsilon_{ij} + m_{ij} \chi_{ij}) d\Omega, \quad i, j = x, y, z, \quad (2)$$

式中 $\varepsilon_{ij}, \sigma_{ij}, \chi_{ij}, m_{ij}$ 分别代表应变张量、Cauchy 应力张量、曲率张量、偶应力张量, 具体定义如下:

$$\varepsilon_{ij} = \frac{1}{2}(u_{i,j} + u_{j,i}), \quad (3)$$

$$\sigma_{ij} = \lambda \varepsilon_{kk} \delta_{ij} + 2G \varepsilon_{ij}, \quad (4)$$

$$\chi_{ij} = \frac{1}{2}(\theta_{i,j} + \theta_{j,i}), \quad (5)$$

$$m_{ij} = 2Gl^2 \chi_{ij}, \quad (6)$$

其中 δ_{ij} 是 Kronecker 符号, l 是内禀特征长度, θ_i 为以下旋转张量分量:

$$\theta_x = \frac{1}{2} \left(\frac{\partial u_z}{\partial y} - \frac{\partial u_y}{\partial z} \right), \theta_y = \frac{1}{2} \left(\frac{\partial u_x}{\partial z} - \frac{\partial u_z}{\partial x} \right), \theta_z = \frac{1}{2} \left(\frac{\partial u_y}{\partial x} - \frac{\partial u_x}{\partial y} \right), \quad (7)$$

λ, G 与弹性模量 E 和 Poisson 比 ν 的关系如下:

$$\lambda = \frac{E\nu}{(1+\nu)(1-2\nu)}, G = \frac{E}{2(1+\nu)}. \quad (8)$$

1.3 准三维功能梯度微梁的运动方程和边界条件

Lee 等^[16]提出的准三维剪切-法向伸缩变形板理论基于如下假设: 1) 板内任一点的面外位移由纯弯曲、纯剪切、法向伸缩产生的挠度组成; 2) 板内任一点面内位移由中面纯拉压、纯弯曲、纯剪切变形产生的面内位移组成; 3) 板内任一点的纯弯曲位移与经典 Kirchhoff 板理论在形式上一致; 4) 板上下表面满足剪切应力为零的条件。

根据文献[16], 准三维梁的位移场可以表示为

$$\begin{cases} u_1(x, z, t) = u(x, t) - z \frac{\partial w_b(x, t)}{\partial x} - f(z) \frac{\partial w_s(x, t)}{\partial x}, u_2(x, z, t) = 0, \\ u_3(x, z, t) = w_b(x, t) + w_s(x, t) + g(z) w_z(x, t), \end{cases} \quad (9)$$

式中 u 是中面纯拉压位移, w_b , w_s 和 w_z 分别是中面纯弯曲、纯剪切和法向伸缩变形产生的挠度. 在准三维剪切变形理论中, 法向伸缩变形由 gw_z 描述, g 反映了法向伸缩变形产生的挠度在梁高度方向的分布形式. 对于 Reddy 型准三维梁, 有

$$f(z) = \frac{4z^3}{3h^2}, \quad g(z) = 1 - \frac{4z^2}{h^2}. \quad (10)$$

准三维功能梯度微梁的应力-应变关系式如下:

$$\begin{Bmatrix} \sigma_x \\ \sigma_z \\ \sigma_{xz} \end{Bmatrix} = \begin{bmatrix} \bar{C}_{11} & \bar{C}_{13} & 0 \\ \bar{C}_{13} & \bar{C}_{11} & 0 \\ 0 & 0 & C_{55} \end{bmatrix} \begin{Bmatrix} \varepsilon_x \\ \varepsilon_z \\ \gamma_{xz} \end{Bmatrix}, \quad (11)$$

式中

$$\bar{C}_{11} = C_{11} - \frac{C_{11}^2}{C_{22}} = \frac{E}{1-\nu^2}, \quad \bar{C}_{13} = C_{13} - \frac{C_{12}C_{23}}{C_{22}} = \frac{E\nu}{1-\nu^2}, \quad C_{55} = \frac{E}{2(1+\nu)}. \quad (12)$$

利用式(2)和式(3)~(6), 可得准三维功能梯度微梁的应变能:

$$\begin{aligned} \Pi_s = & \int_0^L \left[\Sigma_1 \left(\frac{\partial w_s}{\partial x} \right)^2 + \Sigma_2 \left(\frac{\partial^2 w_b}{\partial x^2} \right)^2 + \Sigma_3 \left(\frac{\partial^2 w_s}{\partial x^2} \right)^2 + \Sigma_4 \left(\frac{\partial w_z}{\partial x} \right)^2 + \right. \\ & \Sigma_5 \frac{\partial^2 w_s}{\partial x^2} \frac{\partial^2 w_b}{\partial x^2} + \Sigma_6 \frac{\partial^2 w_s}{\partial x^2} \frac{\partial^2 w_z}{\partial x^2} + \Sigma_7 \frac{\partial w_s}{\partial x} \frac{\partial w_z}{\partial x} + \Sigma_8 w_z^2 + \\ & \Sigma_9 \frac{\partial^2 w_b}{\partial x^2} \frac{\partial u}{\partial x} + \Sigma_{10} w_z \frac{\partial u}{\partial x} + \Sigma_{11} \frac{\partial u}{\partial x} \frac{\partial^2 w_s}{\partial x^2} + \Sigma_{12} w_z \frac{\partial^2 w_s}{\partial x^2} + \\ & \left. \Sigma_{13} \left(\frac{\partial u}{\partial x} \right)^2 + \Sigma_{14} \frac{\partial^2 w_z}{\partial x^2} \frac{\partial^2 w_b}{\partial x^2} + \Sigma_{15} w_z \frac{\partial^2 w_b}{\partial x^2} + \Sigma_{16} \left(\frac{\partial^2 w_z}{\partial x^2} \right)^2 \right] dx, \quad (13) \end{aligned}$$

其中 $\Sigma_1 \sim \Sigma_{16}$ 的表达式如下:

$$\left\{ \begin{aligned} \Sigma_1 &= \int_{-h/2}^{h/2} \left[\frac{8Gl^2 z^2}{h^4} + C_{55} \left(\frac{1}{4} - \frac{2z^2}{h^2} + \frac{4z^4}{h^4} \right) \right] dz, \quad \Sigma_2 = \frac{1}{2} \int_{-h/2}^{h/2} (Gl^2 + z^2 \bar{C}_{11}) dz, \\ \Sigma_3 &= \int_{-h/2}^{h/2} \left(\frac{2Gl^2 z^4}{h^4} + \frac{Gl^2 z^2}{h^2} + \frac{Gl^2}{8} + \frac{8z^6 \bar{C}_{11}}{9h^4} \right) dz, \quad \Sigma_4 = \int_{-h/2}^{h/2} \left[\frac{8Gl^2 z^2}{h^4} + C_{55} \left(\frac{1}{4} - \frac{2z^2}{h^2} + \frac{4z^4}{h^4} \right) \right] dz, \\ \Sigma_5 &= \int_{-h/2}^{h/2} \left(\frac{Gl^2}{2} + \frac{4\bar{C}_{11}^4}{3h^2} + \frac{2Gl^2 z^2}{h^2} \right) dz, \quad \Sigma_6 = \int_{-h/2}^{h/2} \frac{Gl^2}{4} \left(1 - \frac{16z^4}{h^4} \right) dz, \\ \Sigma_7 &= \int_{-h/2}^{h/2} \left[C_{55} \left(\frac{8z^4}{h^4} - \frac{4z^2}{h^2} + \frac{1}{2} \right) - \frac{16Gl^2 z^2}{h^4} \right] dz, \quad \Sigma_8 = \int_{-h/2}^{h/2} \frac{32z^2 \bar{C}_{11}}{h^4} dz, \\ \Sigma_9 &= - \int_{-h/2}^{h/2} \bar{C}_{11} dz, \quad \Sigma_{10} = - \int_{-h/2}^{h/2} \frac{8\bar{C}_{13} z}{h^2} dz, \quad \Sigma_{11} = - \int_{-h/2}^{h/2} \frac{4\bar{C}_{11} z^3}{3h^2} dz, \\ \Sigma_{12} &= \int_{-h/2}^{h/2} \frac{32\bar{C}_{13} z^4}{3h^4} dz, \quad \Sigma_{13} = \int_{-h/2}^{h/2} \frac{\bar{C}_{11}}{2} dz, \quad \Sigma_{14} = \int_{-h/2}^{h/2} \frac{Gl^2}{2} \left(1 - \frac{4z^2}{h^2} \right) dz, \\ \Sigma_{15} &= \int_{-h/2}^{h/2} \frac{8\bar{C}_{13} z^2}{h^2} dz, \quad \Sigma_{16} = \int_{-h/2}^{h/2} Gl^2 \left(\frac{2z^4}{h^4} - \frac{z^2}{h^2} + \frac{1}{8} \right) dz. \end{aligned} \right. \quad (14)$$

根据式(9), 可得准三维功能梯度微梁的动能如下:

$$\Pi_k = \int_{\Omega} \frac{1}{2} \rho(z) \left[\left(\frac{\partial u_1}{\partial t} \right)^2 + \left(\frac{\partial u_2}{\partial t} \right)^2 + \left(\frac{\partial u_3}{\partial t} \right)^2 \right] d\Omega =$$

$$\int_0^L \left[\frac{M_0}{2} \left(\frac{\partial u}{\partial t} \right)^2 - M_1 \frac{\partial u}{\partial t} \frac{\partial^2 w_b}{\partial t \partial x} - \frac{4M_3}{3h^2} \frac{\partial u}{\partial t} \frac{\partial^2 w_s}{\partial t \partial x} + \frac{M_2}{2} \left(\frac{\partial^2 w_b}{\partial t \partial x} \right)^2 + \frac{4M_4}{3h^2} \frac{\partial^2 w_b}{\partial t \partial x} \frac{\partial^2 w_s}{\partial t \partial x} + \frac{8M_6}{9h^4} \left(\frac{\partial^2 w_s}{\partial t \partial x} \right)^2 + \frac{M_0}{2} \left(\frac{\partial w_b}{\partial t} \right)^2 + M_0 \frac{\partial w_b}{\partial t} \frac{\partial w_s}{\partial t} - \frac{4M_2}{h^2} \frac{\partial w_b}{\partial t} \frac{\partial w_z}{\partial t} + \frac{M_0}{2} \left(\frac{\partial w_s}{\partial t} \right)^2 - \frac{4M_2}{h^2} \frac{\partial w_s}{\partial t} \frac{\partial w_z}{\partial t} + \frac{8M_4}{h^4} \left(\frac{\partial w_z}{\partial t} \right)^2 \right] dx, \quad (15)$$

式中

$$(M_0, M_1, M_2, M_3, M_4, M_6) = b \int_{-h/2}^{h/2} \rho(z) (1, z, z^2, z^3, z^4, z^6) dz, \quad \Omega = b \times h \times L. \quad (16)$$

分布荷载 q 作用下的外力功为

$$\Pi_e = \int_0^L q(w_b + w_s + w_z) dx. \quad (17)$$

利用式(13)、(15)、(17)及第二类 Lagrange 方程^[18-19]可得准三维功能梯度微梁的运动微分方程如下:

$$2\Sigma_{13} \frac{\partial^2 u}{\partial x^2} + \Sigma_9 \frac{\partial^3 w_b}{\partial x^3} + \Sigma_{11} \frac{\partial^3 w_s}{\partial x^3} + \Sigma_{10} \frac{\partial w_z}{\partial x} + \frac{4M_3}{3h^2} \frac{\partial^3 w_s}{\partial t^2 \partial x} + M_1 \frac{\partial^3 w_b}{\partial t^2 \partial x} - M_0 \frac{\partial^2 u}{\partial t^2} - q = 0, \quad \text{or} \quad \delta u = 0, \quad x \in (0, L), \quad (18a)$$

$$\left(\frac{4M_2}{h^2} - M_0 \right) \frac{\partial^2 w_z}{\partial t^2} - M_0 \frac{\partial^2 w_s}{\partial t^2} - M_0 \frac{\partial^2 w_b}{\partial t^2} + \frac{4M_4}{3h^2} \frac{\partial^4 w_s}{\partial x^2 \partial t^2} - M_1 \frac{\partial^3 u}{\partial x \partial t^2} + M_2 \frac{\partial^4 w_b}{\partial x^2 \partial t^2} - \Sigma_9 \frac{\partial^3 u}{\partial x^3} - 2\Sigma_2 \frac{\partial^4 w_b}{\partial x^4} - \Sigma_5 \frac{\partial^4 w_s}{\partial x^4} - \Sigma_{15} \frac{\partial^2 w_z}{\partial x^2} - \Sigma_{14} \frac{\partial^4 w_z}{\partial x^4} + q = 0, \quad \text{or} \quad \delta w_b = 0, \quad x \in (0, L), \quad (18b)$$

$$(2\Sigma_1 + \Sigma_7) \frac{\partial^2 w_s}{\partial x^2} + \left(\frac{4M_2}{h^2} - M_0 \right) \frac{\partial^2 w_z}{\partial t^2} - M_0 \frac{\partial^2 w_s}{\partial t^2} + \frac{4M_4}{3h^2} \frac{\partial^4 w_b}{\partial t^2 \partial x^2} - M_0 \frac{\partial^2 w_b}{\partial t^2} - \Sigma_{11} \frac{\partial^3 u}{\partial x^3} - \Sigma_5 \frac{\partial^4 w_b}{\partial x^4} - 2\Sigma_3 \frac{\partial^4 w_s}{\partial x^4} - \Sigma_{12} \frac{\partial^2 w_z}{\partial x^2} - \Sigma_6 \frac{\partial^4 w_z}{\partial x^4} - \frac{4M_3}{3h^2} \frac{\partial^3 u}{\partial t^2 \partial x} + \frac{16M_6}{9h^4} \frac{\partial^4 w_s}{\partial t^2 \partial x^2} + q = 0, \quad \text{or} \quad \delta w_s = 0, \quad x \in (0, L), \quad (18c)$$

$$q - \Sigma_{10} \frac{\partial u}{\partial x} - \Sigma_{15} \frac{\partial^2 w_b}{\partial x^2} - \Sigma_{12} \frac{\partial^2 w_s}{\partial x^2} - M_0 \frac{\partial^2 w_s}{\partial t^2} - M_0 \frac{\partial^2 w_z}{\partial t^2} - M_0 \frac{\partial^2 w_b}{\partial t^2} - \Sigma_{11} \frac{\partial^3 u}{\partial x^3} - \Sigma_5 \frac{\partial^4 w_b}{\partial x^4} - 2\Sigma_3 \frac{\partial^4 w_s}{\partial x^4} - \Sigma_{12} \frac{\partial^2 w_z}{\partial x^2} - \Sigma_6 \frac{\partial^4 w_z}{\partial x^4} + \frac{4M_4}{3h^2} \frac{\partial^4 w_b}{\partial t^2 \partial x^2} - \frac{4M_3}{3h^2} \frac{\partial^3 u}{\partial t^2 \partial x} + \frac{16M_6}{9h^4} \frac{\partial^4 w_s}{\partial t^2 \partial x^2} = 0, \quad \text{or} \quad \delta w_z = 0, \quad x \in (0, L). \quad (18d)$$

准三维功能梯度微梁的边界条件为

$$2\Sigma_{13} \frac{\partial u}{\partial x} + \Sigma_{19} \frac{\partial^2 w_b}{\partial x^2} + \Sigma_{11} \frac{\partial^2 w_s}{\partial x^2} + \Sigma_{10} w_z = 0, \quad \text{or} \quad \delta u = 0, \quad x = 0, L, \quad (19a)$$

$$\frac{4M_4}{3h^2} \frac{\partial^3 w_s}{\partial t^2 \partial x} + M_2 \frac{\partial^3 w_b}{\partial t^2 \partial x} - \Sigma_9 \frac{\partial^2 u}{\partial x^2} - 2\Sigma_2 \frac{\partial^3 w_b}{\partial x^3} - \Sigma_5 \frac{\partial^3 w_s}{\partial x^3} - \Sigma_{15} \frac{\partial w_z}{\partial x} - \Sigma_{14} \frac{\partial^3 w_z}{\partial x^3} - M_1 \frac{\partial^2 u}{\partial t^2} = 0, \quad \text{or} \quad \delta w_b = 0, \quad x = 0, L, \quad (19b)$$

$$\Sigma_9 \frac{\partial u}{\partial x} + 2\Sigma_2 \frac{\partial^2 w_b}{\partial x^2} + \Sigma_5 \frac{\partial^2 w_s}{\partial x^2} + \Sigma_{15} w_z + \Sigma_{14} \frac{\partial^2 w_z}{\partial x^2} = 0, \quad \text{or} \quad \delta \left(\frac{\partial w_b}{\partial x} \right) = 0, \quad x = 0, L, \quad (19c)$$

$$2\Sigma_1 \frac{\partial w_s}{\partial x} + \Sigma_7 \frac{\partial w_z}{\partial x} - \Sigma_{11} \frac{\partial^2 u}{\partial x^2} - \Sigma_5 \frac{\partial^3 w_b}{\partial x^3} - 2\Sigma_3 \frac{\partial^3 w_s}{\partial x^3} - \Sigma_{12} \frac{\partial w_z}{\partial x} - \Sigma_6 \frac{\partial^3 w_z}{\partial x^3} + \frac{4M_4}{3h^2} \frac{\partial^3 w_b}{\partial t^2 \partial x} - \frac{4M_3}{3h^2} \frac{\partial^2 u}{\partial t^2} + \frac{16M_6}{9h^4} \frac{\partial^3 w_s}{\partial t^2 \partial x} = 0, \quad \text{or} \quad \delta w_s = 0, \quad x = 0, L, \quad (19d)$$

$$\Sigma_{11} \frac{\partial u}{\partial x} + \Sigma_5 \frac{\partial^2 w_b}{\partial x^2} + 2\Sigma_3 \frac{\partial^2 w_s}{\partial x^2} + \Sigma_{12} w_z + \Sigma_6 \frac{\partial^2 w_z}{\partial x^2} = 0, \quad \text{or} \quad \delta \left(\frac{\partial w_s}{\partial x} \right) = 0, \quad x = 0, L, \quad (19e)$$

$$\Sigma_7 \frac{\partial w_s}{\partial x} + 2\Sigma_4 \frac{\partial w_z}{\partial x} - \Sigma_{14} \frac{\partial^3 w_b}{\partial x^3} - \Sigma_6 \frac{\partial^3 w_s}{\partial x^3} - 2\Sigma_{16} \frac{\partial^3 w_z}{\partial x^3} = 0, \quad \text{or} \quad \delta w_z = 0, \quad x = 0, L, \quad (19f)$$

$$\Sigma_{14} \frac{\partial^2 w_b}{\partial x^2} + \Sigma_6 \frac{\partial^2 w_s}{\partial x^2} + 2\Sigma_{16} \frac{\partial^2 w_z}{\partial x^2} = 0, \quad \text{or} \quad \delta \left(\frac{\partial w_z}{\partial x} \right) = 0, \quad x = 0, L. \quad (19g)$$

显然,式(18)和(19)中 u, w_b, w_s, w_z 相互耦合,考虑尺度效应使得该模型的控制方程的阶次显著升高,并导致非经典边界条件的出现.位移场变量的 C^1 连续性要求给边值问题的求解带来了极大困难.对于准三维功能梯度简支微梁,可以采用 Navier 法获得静力弯曲和自由振动的解析解.Navier 法假设位移函数和荷载可以表示为

$$\begin{cases} u = \sum_{n=1}^{\infty} A_n e^{j\omega t} \cos(\beta_n x), w_b = \sum_{n=1}^{\infty} B_n e^{j\omega t} \sin(\beta_n x), w_s = \sum_{n=1}^{\infty} C_n e^{j\omega t} \sin(\beta_n x), \\ w_z = \sum_{n=1}^{\infty} D_n e^{j\omega t} \sin(\beta_n x), q = \sum_{n=1}^{\infty} q_n e^{j\omega t} \sin(\beta_n x), \end{cases} \quad (20)$$

其中 $\beta_n = n\pi/L, \omega$ 为固有圆频率.

将式(20)代入式(18a)~(18d)中可得

$$(\mathbf{K}_n - \omega^2 \mathbf{M}_n) \mathbf{D}_n = \mathbf{q}_n, \quad (21)$$

式中

$$\mathbf{K}_n = \begin{bmatrix} 2\Sigma_{13}\beta_n^2 & \Sigma_9\beta_n^3 & \Sigma_{11}\beta_n^3 & -\Sigma_{10}\beta_n \\ \Sigma_9\beta_n^3 & 2\Sigma_2\beta_n^4 & \Sigma_5\beta_n^4 & \beta_n^2(\Sigma_{14}\beta_n^2 - \Sigma_{15}) \\ \Sigma_{11}\beta_n^3 & \Sigma_5\beta_n^4 & 2\beta_n^2(\Sigma_3\beta_n^2 + \Sigma_1) & \beta_n^2(\Sigma_6\beta_n^2 + \Sigma_7 - \Sigma_{12}) \\ -\Sigma_{10}\beta_n & \beta_n^2(\Sigma_{14}\beta_n^2 - \Sigma_{15}) & \beta_n^2(\Sigma_6\beta_n^2 + \Sigma_7 - \Sigma_{12}) & 2(\Sigma_{16}\beta_n^4 + \Sigma_4\beta_n^2 + \Sigma_8) \end{bmatrix},$$

$$\mathbf{M}_n = \begin{bmatrix} M_0 & -M_1\beta_n & -\frac{4M_3\beta_n}{3h^2} & 0 \\ -M_1\beta_n & M_2\beta_n^2 + M_0 & M_0 + \frac{4M_4\beta_n^2}{3h^2} & M_0 - \frac{4M_2}{h^2} \\ -\frac{4M_3\beta_n}{3h^2} & M_0 + \frac{4M_4\beta_n^2}{3h^2} & M_0 + \frac{16M_6\beta_n^2}{9h^4} & M_0 - \frac{4M_2}{h^2} \\ 0 & M_0 - \frac{4M_2}{h^2} & M_0 - \frac{4M_2}{h^2} & \frac{16M_4}{h^4} - \frac{8M_2}{h^2} + M_0 \end{bmatrix}, \quad \mathbf{q}_n = \frac{4q}{n\pi} \begin{bmatrix} 0 \\ 1 \\ 1 \\ 1 \end{bmatrix}, \quad \mathbf{D}_n = \begin{bmatrix} A_n \\ B_n \\ C_n \\ D_n \end{bmatrix}. \quad (22)$$

2 准三维功能梯度微梁的微分求积有限元

本节汲取微分求积法和有限元法的优点,构造一种对应于准三维功能梯度微梁的微分求积有限元.该方法采用弱形式描述微梁的边值问题,在进行求解域划分后通过 Gauss-Lobatto 求积准则与微分求积准则的融合来离散子域内势能和动能泛函.如前所述,本文模型所涉及的四个位移场变量均具有 C^1 连续性要求,因此

单元交界处需要引入位移场变量的 1 阶导数.单元势能和动能泛函离散过程中需使用 4 个微分求积点和 Gauss-Lobatto 求积点.根据文献[18-19],构造如图 2 所示的微分求积几何映射策略.

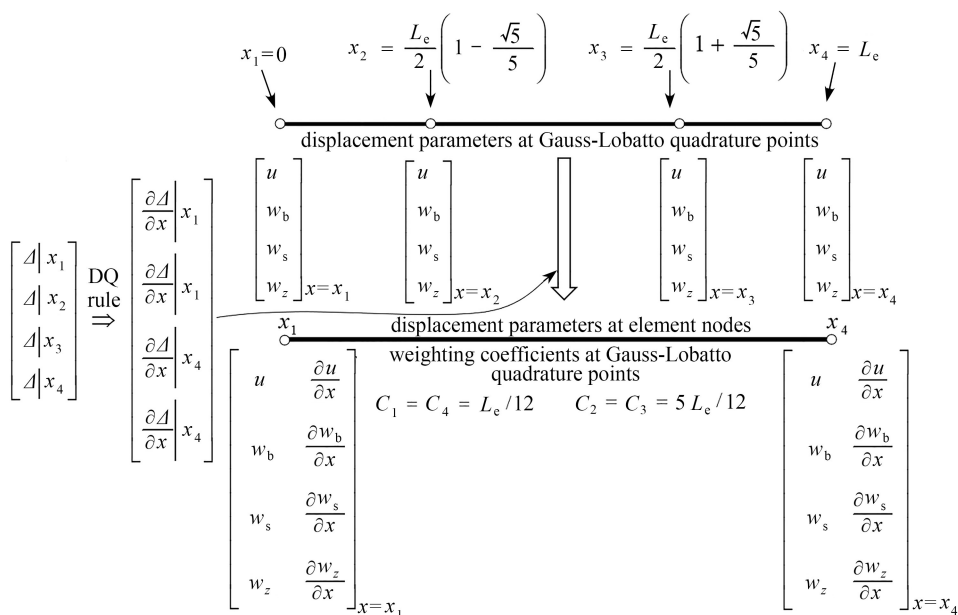


图 2 准三维功能梯度微梁的微分求积几何映射策略

Fig. 2 The differential quadrature-based geometric mapping scheme for the quasi-3D FG microbeam model

根据图 2 中映射关系,采用 Lagrange 插值技术构造位移场变量 Δ 的试函数如下:

$$\Delta = \sum_{i=1}^4 l_i(x)\Delta_i, \tag{23}$$

其中 Δ 表示位移场变量 u, w_b, w_s 和 w_z, Δ_i 和 $l_i(x)$ 分别表示位移场变量在第 i 个求积点处的函数值和 Lagrange 插值函数.对于长度为 L_e 的梁单元,求积点坐标为

$$x_1 = 0, x_2 = \frac{L_e}{2} \left(1 - \frac{\sqrt{5}}{5} \right), x_3 = \frac{L_e}{2} \left(1 + \frac{\sqrt{5}}{5} \right), x_4 = L_e. \tag{24}$$

采用微分求积准则,可将求积点处导数表示为以下矩阵形式:

$$\mathbf{\Delta}_G^{(0)} = \mathbf{A}_0 \mathbf{\Delta}_G, \mathbf{\Delta}_G^{(1)} = \mathbf{A}_1 \mathbf{\Delta}_G, \mathbf{\Delta}_G^{(2)} = \mathbf{A}_2 \mathbf{\Delta}_G, \tag{25}$$

其中 $\mathbf{\Delta}_G^{(m)}$ 表示所有求积点处位移场变量 Δ 的 m 阶导数值组成的列向量,即

$$\mathbf{\Delta}_G^{(m)} = \left[\left(\frac{\partial^m \Delta}{\partial x^m} \right)_1, \left(\frac{\partial^m \Delta}{\partial x^m} \right)_2, \left(\frac{\partial^m \Delta}{\partial x^m} \right)_3, \left(\frac{\partial^m \Delta}{\partial x^m} \right)_4 \right]^T, \tag{26}$$

矩阵 $\mathbf{A}_0, \mathbf{A}_1, \mathbf{A}_2$ 的表达式见文献[18-19].

显然,式(25)中三个表达式的右侧仅包含位移场变量在求积点处的函数值本身,而没有涉及函数的 1 阶导数.为了满足 C^1 连续性要求,需将求积点处函数值变换为单元节点参数.为此,定义下列节点位移向量 $\mathbf{\Delta}_N$:

$$\mathbf{\Delta}_N = \left[\Delta_1, \left(\frac{\partial \Delta}{\partial x} \right)_1, \Delta_4, \left(\frac{\partial \Delta}{\partial x} \right)_4 \right]^T. \tag{27}$$

由微分求积准则,可得 $\mathbf{\Delta}_G$ 和 $\mathbf{\Delta}_N$ 之间的关系:

$$\mathbf{\Delta}_N = \mathbf{B} \mathbf{\Delta}_G, \tag{28}$$

矩阵 \mathbf{B} 的表达式见文献[18-19].

利用式(25)和式(28),梁单元的应变能、动能、外力功被离散为

$$\begin{aligned} \Pi_s = & \mathbf{w}_{Ns}^T (\mathbf{B}^{-1})^T [\Sigma_1 (\mathbf{A}_1)^T \mathbf{C}_G \mathbf{A}_1 + \Sigma_3 (\mathbf{A}_2)^T \mathbf{C}_G \mathbf{A}_2] \mathbf{B}^{-1} \mathbf{w}_{Ns} + \\ & \Sigma_2 \mathbf{w}_{Nb}^T (\mathbf{B}^{-1})^T (\mathbf{A}_2)^T \mathbf{C}_G \mathbf{A}_2 \mathbf{B}^{-1} \mathbf{w}_{Nb} + \Sigma_{13} \mathbf{u}_N^T (\mathbf{B}^{-1})^T (\mathbf{A}_1)^T \mathbf{C}_G \mathbf{A}_1 \mathbf{B}^{-1} \mathbf{u}_N + \\ & \mathbf{w}_{Nz}^T (\mathbf{B}^{-1})^T [\Sigma_4 (\mathbf{A}_1)^T \mathbf{C}_G \mathbf{A}_1 + \Sigma_{16} (\mathbf{A}_2)^T \mathbf{C}_G \mathbf{A}_2 + \Sigma_8 \mathbf{C}_G] \mathbf{B}^{-1} \mathbf{w}_{Nz} + \end{aligned}$$

$$\begin{aligned} & \mathbf{w}_{N_z}^T (\mathbf{B}^{-1})^T [\Sigma_{14} (\mathbf{A}_2)^T \mathbf{C}_G \mathbf{A}_2 + \Sigma_{15} (\mathbf{A}_0)^T \mathbf{C}_G \mathbf{A}_2] \mathbf{B}^{-1} \mathbf{w}_{N_b} + \\ & \mathbf{w}_{N_s}^T (\mathbf{B}^{-1})^T [\Sigma_6 (\mathbf{A}_2)^T \mathbf{C}_G \mathbf{A}_2 + \Sigma_7 (\mathbf{A}_1)^T \mathbf{C}_G \mathbf{A}_1 + \Sigma_{12} (\mathbf{A}_2)^T \mathbf{C}_G] \mathbf{B}^{-1} \mathbf{w}_{N_z} + \\ & \Sigma_9 \mathbf{w}_{N_b}^T (\mathbf{B}^{-1})^T (\mathbf{A}_2)^T \mathbf{C}_G \mathbf{A}_1 \mathbf{B}^{-1} \mathbf{u}_N + \Sigma_5 \mathbf{w}_{N_s}^T (\mathbf{B}^{-1})^T (\mathbf{A}_2)^T \mathbf{C}_G \mathbf{A}_2 \mathbf{B}^{-1} \mathbf{w}_{N_b} + \\ & \Sigma_{10} \mathbf{w}_{N_z}^T (\mathbf{B}^{-1})^T \mathbf{C}_G \mathbf{A}_1 \mathbf{B}^{-1} \mathbf{u}_N + \Sigma_{11} \mathbf{w}_{N_s}^T (\mathbf{B}^{-1})^T (\mathbf{A}_2)^T \mathbf{C}_G \mathbf{A}_1 \mathbf{B}^{-1} \mathbf{u}_N, \end{aligned} \quad (29)$$

$$\begin{aligned} \Pi_k = & \frac{M_0}{2} \dot{\mathbf{u}}_N^T (\mathbf{B}^{-1})^T \mathbf{C}_G \mathbf{B}^{-1} \dot{\mathbf{u}}_N - M_1 \dot{\mathbf{u}}_N^T (\mathbf{B}^{-1})^T \mathbf{C}_G \mathbf{A}_1 \mathbf{B}^{-1} \dot{\mathbf{w}}_{N_b} - \frac{4M_3}{3h^2} \dot{\mathbf{u}}_N^T (\mathbf{B}^{-1})^T \mathbf{C}_G \mathbf{A}_1 \mathbf{B}^{-1} \dot{\mathbf{w}}_{N_s} + \\ & \frac{1}{2} \dot{\mathbf{w}}_{N_b}^T (\mathbf{B}^{-1})^T (M_2 \mathbf{A}_1^T \mathbf{C}_G \mathbf{A}_1 + M_0 \mathbf{C}_G) \mathbf{B}^{-1} \dot{\mathbf{w}}_{N_b} + \dot{\mathbf{w}}_{N_b}^T (\mathbf{B}^{-1})^T \left(\frac{4M_4}{3h^2} \mathbf{A}_1^T \mathbf{C}_G \mathbf{A}_1 + M_0 \mathbf{C}_G \right) \mathbf{B}^{-1} \dot{\mathbf{w}}_{N_s} + \\ & \dot{\mathbf{w}}_{N_s}^T (\mathbf{B}^{-1})^T \left(\frac{8M_6}{9} \mathbf{A}_1^T \mathbf{C}_G \mathbf{A}_1 + \frac{M_0 \mathbf{C}_G}{2} \right) \mathbf{B}^{-1} \dot{\mathbf{w}}_{N_s} + \frac{8M_4}{h^4} \dot{\mathbf{w}}_{N_z}^T (\mathbf{B}^{-1})^T \mathbf{C}_G \mathbf{B}^{-1} \dot{\mathbf{w}}_{N_z} - \\ & \frac{4M_2}{h^2} [\dot{\mathbf{w}}_{N_b}^T (\mathbf{B}^{-1})^T \mathbf{C}_G \mathbf{B}^{-1} \dot{\mathbf{w}}_{N_z} + \dot{\mathbf{w}}_{N_s}^T (\mathbf{B}^{-1})^T \mathbf{C}_G \mathbf{B}^{-1} \dot{\mathbf{w}}_{N_z}], \end{aligned} \quad (30)$$

$$\Pi_e = (\mathbf{w}_{N_b}^T + \mathbf{w}_{N_s}^T + \mathbf{w}_{N_z}^T) (\mathbf{B}^{-1})^T \mathbf{C}_G \mathbf{q}_G. \quad (31)$$

权系数矩阵 \mathbf{C}_G 和求积点荷载列向量如下:

$$\mathbf{C}_G = \frac{L_e}{12} \text{diag}[1, 5, 5, 1], \quad \mathbf{q}_G = [q_1, q_2, q_3, q_4]^T. \quad (32)$$

引入下列单元总体节点列向量:

$$\begin{aligned} \mathbf{d}_N = & \left[(u)_1, \left(\frac{\partial u}{\partial x} \right)_1, (w_b)_1, \left(\frac{\partial w_b}{\partial x} \right)_1, (w_s)_1, \left(\frac{\partial w_s}{\partial x} \right)_1, (w_z)_1, \left(\frac{\partial w_z}{\partial x} \right)_1, \right. \\ & \left. (u)_4, \left(\frac{\partial u}{\partial x} \right)_4, (w_b)_4, \left(\frac{\partial w_b}{\partial x} \right)_4, (w_s)_4, \left(\frac{\partial w_s}{\partial x} \right)_4, (w_z)_4, \left(\frac{\partial w_z}{\partial x} \right)_4 \right]^T. \end{aligned} \quad (33)$$

由最小势能原理, 可得单元刚度矩阵 \mathbf{K}^e 、质量矩阵 \mathbf{M}^e 、荷载列向量 \mathbf{F}^e 的元素如下:

$$K_{ij}^e = \frac{\partial^2 \Pi_s}{\partial d_i \partial d_j}, \quad M_{ij}^e = \frac{\partial^2 \Pi_k}{\partial d_i \partial d_j}, \quad F_i^e = \frac{\partial \Pi_e}{\partial d_i}, \quad (34)$$

其中 d_i 表示 \mathbf{d}_N 中第 i 个元素, K_{ij}^e 和 M_{ij}^e 表示刚度矩阵 \mathbf{K}^e 和质量矩阵 \mathbf{M}^e 的具体元素.

梁端部常见约束可以分为简支(S)、固支(C)、自由(F)三种类型.对于简支-简支(SS)、固支-固支(CC)、固支-自由(CF)梁,相应的边界条件如下:

$$\text{SS:} \quad u|_{x=0} = w_b|_{x=0,L} = w_s|_{x=0,L} = w_z|_{x=0,L} = 0; \quad (35)$$

$$\text{CC:} \quad u|_{x=0,L} = w_b|_{x=0,L} = w_s|_{x=0,L} = w_z|_{x=0,L} = \frac{\partial w_b}{\partial x} \Big|_{x=0,L} = \frac{\partial w_s}{\partial x} \Big|_{x=0,L} = \frac{\partial w_z}{\partial x} \Big|_{x=0,L} = 0; \quad (36)$$

$$\text{CF:} \quad u|_{x=0} = w_b|_{x=0} = w_s|_{x=0} = w_z|_{x=0} = \frac{\partial w_b}{\partial x} \Big|_{x=0} = \frac{\partial w_s}{\partial x} \Big|_{x=0} = \frac{\partial w_z}{\partial x} \Big|_{x=0} = 0. \quad (37)$$

3 数值算例分析

本节对功能梯度微梁的静力弯曲和自由振动进行算例分析,借此验证理论模型及数值方法的有效性.为了与现有文献比较,考虑 $\text{Al}_2\text{O}_3/\text{Al}$ 和 SiC/Al 两类微梁,相应的组分材料参数由表 1 列出.类似于文献[5-7, 12],内禀特征长度设为 $l = 15 \mu\text{m}$, 于是 h/l 表示无量纲厚度.为便于后续研究,引入下述无量纲参数:

$$\begin{cases} \bar{w}(x, z) = \frac{100E_m b h^3}{12qL^4} w(x, z), \quad \bar{\sigma}_x(x, z) = \frac{bh}{qL} \sigma_x(x, z), \quad \bar{\tau}_{xy}(x, z) = \frac{bh}{qL} \tau_{xy}(x, z), \\ \bar{\omega}_n = \omega_n L^2 \sqrt{\rho_m/E_m}/h. \end{cases} \quad (38)$$

表 1 功能梯度微梁组分材料参数
Table 1 Material parameters of FG microbeams

material	E / GPa	ν	$\rho / (\text{kg/m}^3)$
Al	70	0.3	2 702
Al_2O_3	380	0.3	3 960
SiC	427	0.17	3 100

3.1 有效性验证

表 2 给出了三种方法所预测的受均布荷载 q 作用的 $\text{Al}_2\text{O}_3/\text{Al}$ 功能梯度简支微梁跨中无量纲中面挠度 \bar{w}_{\max} 。本文所构造的微分求积有限元 (differential quadrature finite element, DQFEM) 和文献 [10] 中 FEM 均采用 6 个单元。需要说明的是,在相同节点参数下,对应于同一微梁模型的 DQFEM 和 FEM 刚度矩阵和荷载向量是相同的,两者的质量矩阵虽然具有相同的结构,但对应的元素不同,这点在文献 [18-19] 中已有验证。因此,在梁的静力弯曲分析中,DQFEM 和 FEM 的收敛性相同。从表 2 可以看出,DQFEM 与 FEM 的预测结果与 Navier 级数解十分吻合。此外, h/l 减小或者 L/h 的增大会导致 \bar{w}_{\max} 减小,这说明忽略尺度效应会低估结构刚度,而忽略剪切变形效应则相反。

表 2 不同梯度指数下功能梯度简支微梁的无量纲中面挠度
Table 2 The dimensionless central deflections of the SS FG microbeam for various gradient indexes

n	method	$L/h = 5$				$L/h = 10$			
		$h/l = 8$	$h/l = 4$	$h/l = 2$	$h/l = 1$	$h/l = 8$	$h/l = 4$	$h/l = 2$	$h/l = 1$
0	DQFEM	0.213 6	0.173 4	0.099	0.036 4	0.201 6	0.164 6	0.094 9	0.035 2
	FEM ^[10]	0.213 6	0.173 4	0.099	0.036 4	0.201 6	0.164 6	0.094 9	0.035 2
	Navier	0.213 6	0.173 4	0.099	0.036 4	0.201 6	0.164 6	0.094 9	0.035 2
1	DQFEM	0.426 9	0.339 1	0.186 1	0.066 3	0.405 8	0.733 1	0.179 2	0.064 2
	FEM ^[10]	0.426 8	0.339 1	0.186 1	0.066 3	0.405 7	0.733 0	0.179 2	0.064 2
	Navier	0.426 9	0.339 1	0.186 1	0.066 3	0.405 3	0.733 2	0.179 2	0.064 2
10	DQFEM	0.800 8	0.666 9	0.402 0	0.156 5	0.323 9	0.619 6	0.383 3	0.152 1
	FEM ^[10]	0.800 8	0.666 9	0.402 0	0.156 5	0.323 8	0.619 5	0.383 3	0.152 1
	Navier	0.801 0	0.667 0	0.402 1	0.156 5	0.323 9	0.619 6	0.383 3	0.152 1

表 3 给出了 DQFEM 和 FEM 所预测的 $\text{Al}_2\text{O}_3/\text{Al}$ 功能梯度简支微梁的 1 阶、5 阶、15 阶无量纲固有频率。此处, $L/h = 5, h/l = 1$ 和 $n = 1$ 。从表 3 可以看出,两种方法所得的 1 阶固有频率迅速收敛,随着模态阶次的升高,相应固有频率的收敛性有所降低。对于高阶固有频率,DQFEM 的收敛性明显好于 FEM。为了解释 DQFEM 的计算效率优势,图 3 比较了 DQFEM 和 FEM 在分析功能梯度简支微梁自由振动时所对应的质量矩阵(消除边界约束后)条件数的对数。此处, $L/h = 5, h/l = 1$ 和 $n = 1, 10$ 。结果显示,DQFEM 所对应的质量矩阵条件数明显小于 FEM 所对应的质量矩阵条件数,说明 DQFEM 的质量矩阵更良态,因而在分析振动问题时具有更高的计算效率。原因在于 DQFEM 和 FEM 在节点配置上存在差异,DQFEM 选取 Gauss-Lobatto 求积点为节点,在减少额外插值计算的同时也提高了计算效率,同时通过 DQ 准则来直接离散近似函数在积分点处的导数值。文献 [19-20] 针对各向同性应变梯度 Mindlin 板和 Kirchhoff 板的微分求积有限元的计算效率也进行过类似的分析。

表 3 不同单元数目下功能梯度微梁的 1 阶、5 阶、15 阶无量纲固有频率
Table 3 The 1st, 5th and 15th dimensionless frequencies of the SS FG microbeam under various numbers of elements

N	$\bar{\omega}_1$		$\bar{\omega}_5$		$\bar{\omega}_{15}$	
	DQFEM	FEM	DQFEM	FEM	DQFEM	FEM
4	10.224 0	10.224 0	64.623 6	64.637 9	170.441 0	173.455 0
8	10.221 5	10.221 5	64.548 5	64.548 8	169.147 5	169.149 7
12	10.221 3	10.221 3	64.539 5	64.541 1	169.091 8	169.092 0
16	10.221 3	10.221 3	64.539 1	64.539 5	169.078 9	169.081 8
20	10.221 3	10.221 3	64.539 1	64.539 1	169.078 9	169.078 9

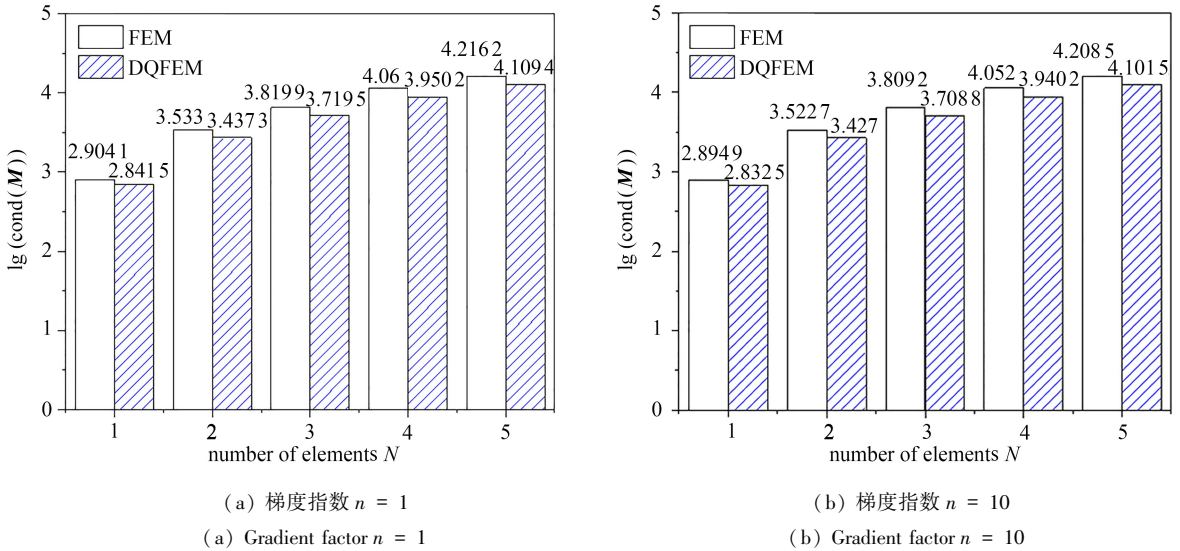


图3 DQFEM和FEM所对应的质量矩阵条件数的比较

Fig. 3 Comparison of the common logarithm condition numbers of the DQFEM and the FEM

3.2 功能梯度微梁的静力弯曲分析

图4绘制了不同梯度指数下长度为 L 、截面为 $h \times h$ 的SiC/Al功能梯度简支微梁跨中横截面上无量纲正应力沿高度方向的分布.此处采用10个单元计算,长细比设为 $L/h = 10$.图中结果显示,当 $n = 0$ 时,正应力沿高度方向线性变化,原因在于梁由纯陶瓷组成,当 $n > 0$ 时,材料性能的非均匀性使得正应力与高度呈现出非线性关系.当 $n = 1$ 时,梁中陶瓷成分较多且由下到上呈梯度递减趋势,在靠近梁上侧面附近,陶瓷成分较少且材料成分变化趋势最小,所以无量纲正应力曲线呈现出下半侧变化明显,上半侧趋于平滑;当 $n = 10$ 时,梁中金属成分较多且从上到下梯度递减,在靠近梁上侧面附近,金属成分最多且材料成分变化趋势最大,所以 $n = 10$ 时的无量纲正应力变化曲线与 $n = 1$ 时变化曲线呈相反趋势.从图中还可以发现, $h/l = 8$ 时的无量纲正应力明显大于 $h/l = 1$ 时的情形,原因在于内禀特征长度的增加使微梁刚性增强,因而结构的变形程度和应力均会降低.

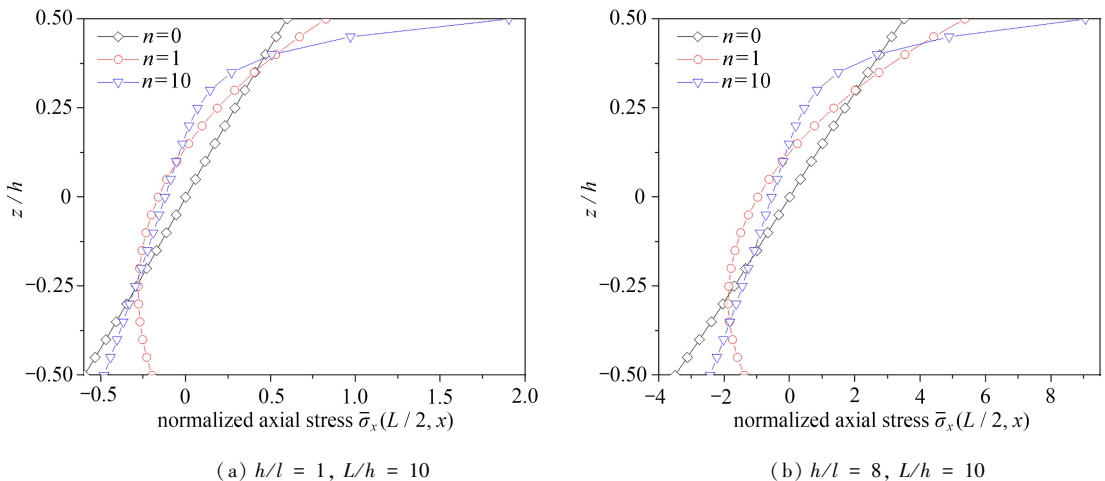


图4 不同梯度指数下功能梯度简支微梁跨中横截面上无量纲正应力沿高度方向的分布

Fig. 4 The through-the-thickness distribution of dimensionless normal stresses in the SS FG microbeam under various gradient factors

表4给出了对应于不同梯度指数和无量纲厚度的横截面切应力 $\bar{\tau}_{xy}(0,0)$.从表中可以看出,随着 h/l 的增大,无量纲切应力随之增大;随着梯度指数 n 的增大,无量纲切应力随之减小;DQFEM所预测结果与Navier级数解十分接近.

表 4 功能梯度简支微梁的无量纲切应力 $\bar{\tau}_{xy}(0,0)$

Table 4 Dimensionless shear stresses $\bar{\tau}_{xy}(0,0)$ in the SS FG microbeam

h/l	$n = 0$			$n = 1$			$n = 10$		
	DQFEM	Navier	relative error $\delta / \%$	DQFEM	Navier	relative error $\delta / \%$	DQFEM	Navier	relative error $\delta / \%$
∞	0.719 2	0.724 0	-0.661 8	0.709 9	0.719 9	-1.383 9	0.627 2	0.628 1	-0.139 0
8	0.654 8	0.658 2	-0.509 6	0.641 6	0.651 3	-1.491 0	0.550 8	0.555 3	-0.815 0
4	0.520 4	0.524 0	-0.695 0	0.505 3	0.513 6	-1.619 9	0.411 0	0.414 3	-0.792 5
2	0.290 6	0.292 6	-0.686 0	0.279 6	0.284 0	-1.533 1	0.197 3	0.199 0	-0.865 4
1	0.106 0	0.106 4	-0.380 9	0.101 8	0.103 6	-1.722 3	0.060 1	0.060 2	-0.101 0

表 5 分别列出了长度为 L 、截面为 $h \times h$ 的 Al_2O_3/Al 功能梯度微梁在 SS 和 CC 边界下的无量纲最大挠度 $100E_m b h^3 w(L/2,0)/(qL^4)$ 。表中结果显示,当梯度指数 n 或者 h/l 增加时,无量纲挠度也增大,这是因为两个参数的增大均会导致梁的刚度减小。此外,无量纲挠度随着长细比 L/h 的增大而减小。

表 5 不同梯度指数下功能梯度微梁的无量纲最大挠度

Table 5 The maximum dimensionless deflections of the SS and CC FG microbeams for various parameters

boundary type	L/h	n	h/l				
			∞	8	4	2	1
SS	5	0	3.204 3	2.978 8	2.459 7	1.450 4	0.551 6
		1	6.242 9	5.739 6	4.622 1	2.600 4	0.950 0
		10	10.984 1	10.258	8.574 4	5.207 6	2.047 3
		0	2.959 8	2.758 3	2.290 5	1.364 8	0.521 7
		1	5.830 0	5.371 9	4.347 1	2.465 7	0.903 1
		10	9.868 1	9.274 9	7.860 9	4.891 8	1.952 9
	10	0	2.898 7	2.703 1	2.248 1	1.343 5	0.514 8
		1	5.726 8	5.279 8	4.278 1	2.432 2	0.892 3
		10	9.588 9	9.028 1	7.681 5	4.813 4	1.931 5
		0	0.858 5	0.789 7	0.645 2	0.386 0	0.161 6
		1	1.613 5	1.472 3	1.182 4	0.686 5	0.279 9
		10	3.210 7	2.910 7	2.312 6	1.323 8	0.534 3
CC	10	0	0.644 7	0.598 2	0.496 0	0.301 1	0.123 8
		1	1.252 4	1.150 7	0.933 1	0.543 8	0.215 8
		10	2.223 8	2.067 5	1.722 6	1.056 8	0.435 1
	20	0	0.591 6	0.550 6	0.458 0	0.277 2	0.111 2
		1	1.162 7	1.070 6	0.869 0	0.502 3	0.193 6
		10	1.974 6	1.852 3	1.568 8	0.983 4	0.404 2

3.3 功能梯度微梁的自由振动分析

本节利用准三维梁模型分析长度为 L 、截面为 $h \times h$ 的 Al_2O_3/Al 功能梯度微梁的自由振动。此处采用 32 个单元,假定 $L/h = 5$ 和 $h/l = \infty$ (即不考虑尺度效应)。表 6 给出了不同梯度指数下 DQFEM 与文献[21]中 FEM 所预测的 1 阶固有频率,从表中可以看到两种方法所得结果吻合得很好。

表 6 功能梯度简支微梁的 1 阶无量纲固有频率

Table 6 The 1st dimensionless natural frequencies of the SS FG microbeam

method	n					
	0	0.5	1	2	5	10
FEM ^[21]	5.161 8	4.424 0	4.007 9	3.644 2	3.413 3	3.290 3
DQFEM	5.161 6	4.425 3	4.009 4	3.645 1	3.410 9	3.286 6

表 7 列出了不同无量纲厚度下功能梯度悬臂微梁的前 10 阶无量纲固有频率。此处 $L/h = 20, n = 1$ 。表中结果显示,尺度效应对微梁固有频率具有显著影响,当 $h/l = 1$ 时尺度效应最强,当 $h/l > 20$ 时尺度效应对固

有频率的影响几乎可以忽略。

表7 功能梯度悬臂微梁的前10阶无量纲固有频率

Table 7 The first 10 dimensionless natural frequencies of the CF FG microbeam

mode	h/l						
	1	2	4	8	20	40	100
1	3.824 1	2.328 7	1.758 6	1.583 6	1.530 9	1.523 2	1.521 1
2	23.788 6	14.467 7	10.914 7	9.823 2	9.494 7	9.446 8	9.433 4
3	53.424 5	39.978 3	30.109 2	27.073 3	26.159 1	26.025 8	25.988 4
4	65.846 4	53.407 6	53.334 1	51.714 3	50.035 9	49.783 6	49.712 5
5	126.984 9	76.969 6	57.891 8	53.604 0	53.500 6	53.493 1	53.491 2
6	160.229 3	124.532 3	93.287 6	83.621 4	80.703 1	80.277 3	80.157 7
7	205.975 4	160.257 5	135.757 0	121.432 9	117.100 2	116.467 7	116.290 0
8	266.881 7	181.877 2	160.111 8	159.625 9	157.498 7	156.829 1	156.629 3
9	301.304 1	248.159 0	184.585 4	165.163 8	161.252 1	161.039 4	160.991 3
10	373.402 8	266.882 8	238.622 6	212.380 4	204.384 3	203.214 9	202.886 2

图5研究了梯度指数和无量纲厚度对功能梯度简支微梁的1阶振动频率的影响,此处 $L/h = 10$ 。为比较起见,图5同时给出了对应的 Navier 级数解。从图中可以看出,数值解和解析解呈现出很好的一致性;随着 n 或 h/l 的增大,1阶无量纲固有频率随之减小,这是由于两个参数的增加均会引起结构刚度减小。

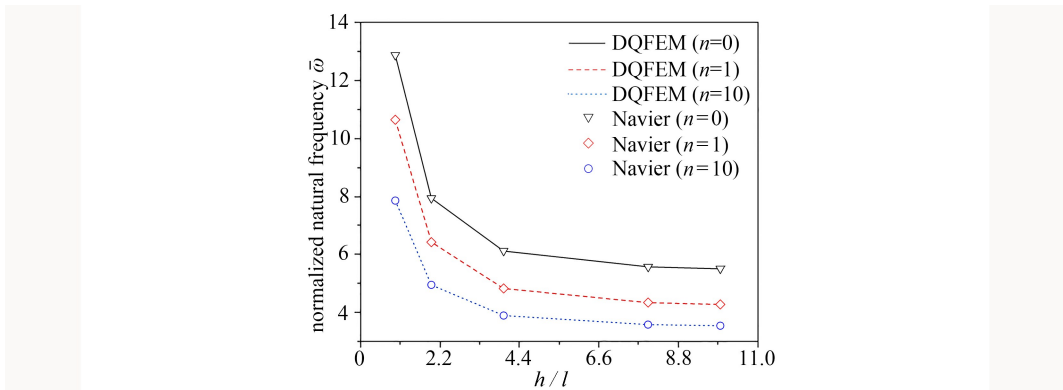
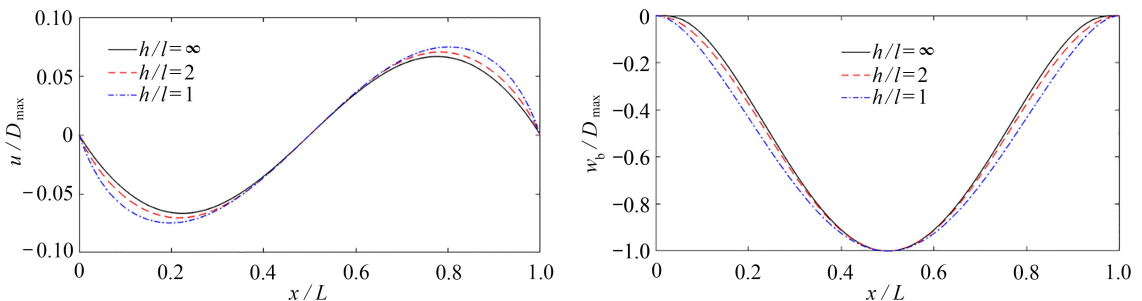


图5 功能梯度简支微梁在不同梯度指数下的1阶无量纲固有频率

Fig. 5 The 1st dimensionless natural frequencies of the SS FG microbeam with different gradient indexes

图6绘制了不同无量纲厚度下功能梯度固支微梁的1阶振动模态,此处 $L/h = 4$ 和 $n = 1$ 。从图6可以看出,尺度效应对 u 和 w_b 的振动模态影响比较小,而对 w_s 和 w_z 的振动模态影响显著;尺度效应会增强 u, w_z, w_b 对应的振动模态,而抑制 w_s 对应的振动模态,原因在于尺度效应和剪切变形效应对梁的刚度起着相反的作用。图7绘制了不同梯度指数下功能梯度固支微梁的1阶振动模态,此处 $L/h = 4$ 和 $h/l = 0.5$ 。图7结果显示,梯度指数对 u, w_z, w_s 对应的1阶振动模态影响显著,而对 w_b 对应的1阶振动模态几乎没有影响;功能梯度指数对法向伸缩变形的影响特别明显。如前所述,功能梯度微梁的轴向振动和弯曲振动的相互耦合会引起位移分量 u, w_z, w_b, w_s 所对应的振动模态此消彼长。 D_{\max} 为4个模态位移列向量中绝对值的最大值。



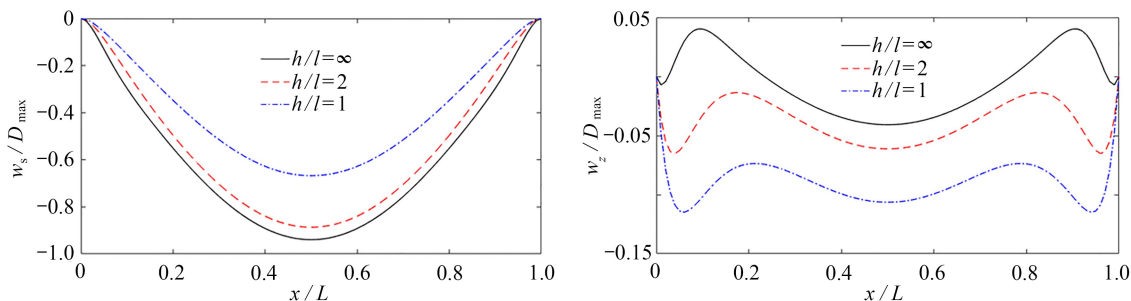


图 6 尺度效应对两端固支功能梯度微梁的 1 阶振动模式的影响

Fig. 6 Size effects on the 1st mode shapes of the CC FG microbeam

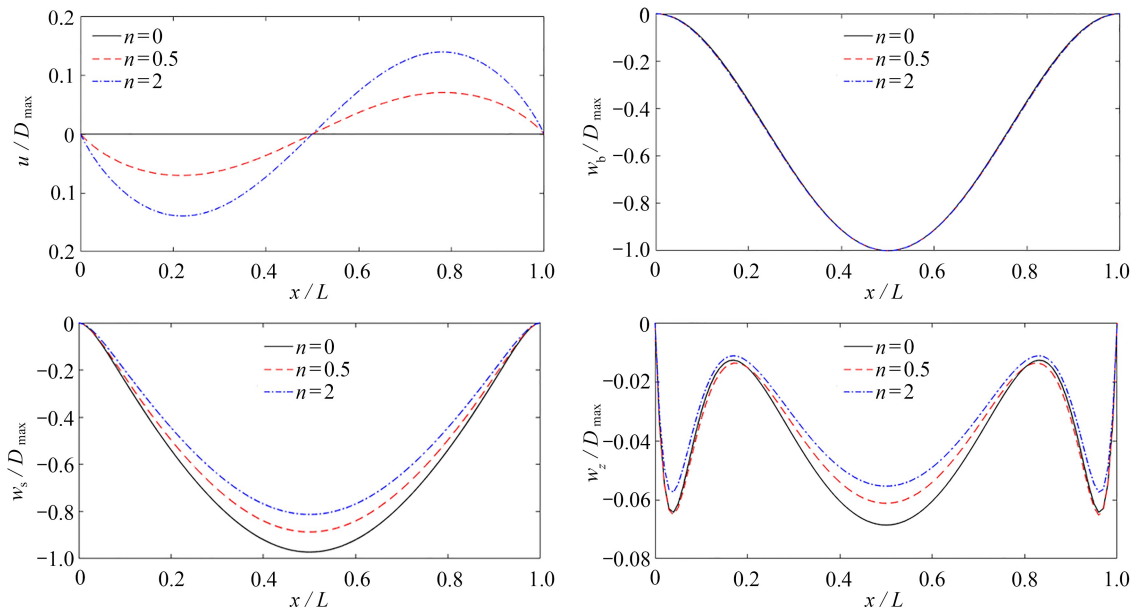


图 7 梯度指数对两端固支功能梯度微梁的 1 阶振动模式的影响

Fig. 7 Effects of the gradient index on the 1st mode shapes of the CC FG microbeam

4 结 论

本文将修正的偶应力理论与四参数高阶剪切-法向伸缩变形理论相结合发展出一种准三维功能梯度微梁模型,采用第二类 Lagrange 方程推导了微梁的运动方程和边界条件,构造了一种 2 节点 16 自由度微分求积有限元求解相应的静动力学边值问题.通过对比性研究,验证了本文梁模型及梁单元的有效性.最后,研究了各参数以及边界条件对微梁静态响应与振动特性的影响.结果表明:相比于标准的 C^1 梁单元,本文微分求积有限元具有更好的收敛性;增大内禀特征长度或者减小梯度指数均会提高微梁的刚度,从而使梁的静态响应幅值降低、振动频率增加;随着长细比的减小,法向伸缩变形和高阶剪切变形效应显著增强;尺度效应和梯度指数不仅影响微梁的静态响应和振动频率,还会显著改变微梁的振动模式.

参考文献 (References):

- [1] LAM D C C, YANG F, CHONG A C M, et al. Experiments and theory in strain gradient elasticity[J]. *Journal of the Mechanics and Physics of Solids*, 2003, **51**(8): 1477-1508.
- [2] LI Z, HE Y, LEI J, et al. A standard experimental method for determining the material length scale based on modified couple stress theory[J]. *International Journal of Mechanical Sciences*, 2018, **141**: 198-205.
- [3] LIU D, HE Y, TANG X, et al. Size effects in the torsion of microscale copper wires: experiment and analysis [J]. *Scripta Materialia*, 2012, **66**(6): 406-409.

- [4] YANG F, CHONG A C M, LAM D C C, et al. Couple stress based strain gradient theory for elasticity[J]. *International Journal of Solids and Structures*, 2002, **39**(10): 2731-2743.
- [5] ZHANG B, HE Y, LIU D, et al. An efficient size-dependent plate theory for bending, buckling and free vibration analyses of functionally graded microplates resting on elastic foundation[J]. *Applied Mathematical Modelling*, 2015, **39**(13): 3814-3845.
- [6] ZHANG B, HE Y, LIU D, et al. A size-dependent third-order shear deformable plate model incorporating strain gradient effects for mechanical analysis of functionally graded circular/annular microplates[J]. *Composites (Part B): Engineering*, 2015, **79**: 553-580.
- [7] LEI J, HE Y, ZHANG B, et al. A size-dependent FG micro-plate model incorporating higher-order shear and normal deformation effects based on a modified couple stress theory[J]. *International Journal of Mechanical Sciences*, 2015, **104**: 8-23.
- [8] NGUYEN H X, NGUYEN T N, ABDEL-WAHAB M, et al. A refined quasi-3D isogeometric analysis for functionally graded microplates based on the modified couple stress theory[J]. *Computer Methods in Applied Mechanics and Engineering*, 2017, **313**: 904-940.
- [9] 杨子豪, 贺丹. 基于精化锯齿理论的功能梯度夹心微板静弯曲模型[J]. 计算力学学报, 2018, **35**(6): 757-762. (YANG Zihao, HE Dan. Static bending model of functionally graded sandwich micro-plates based on the refined zigzag theory[J]. *Chinese Journal of Computational Mechanics*, 2018, **35**(6): 757-762. (in Chinese))
- [10] KARAMANLI A, VO T P. Size dependent bending analysis of two directional functionally graded microbeams via a quasi-3D theory and finite element method[J]. *Composites (Part B): Engineering*, 2018, **144**: 171-183.
- [11] 周博, 郑雪瑶, 康泽天, 等. 基于修正偶应力理论的 Timoshenko 微梁模型和尺寸效应研究[J]. 应用数学和力学, 2019, **40**(12): 1321-1334. (ZHOU Bo, ZHENG Xueyao, KANG Zetian, et al. A Timoshenko micro-beam model and its size effects based on the modified couple stress theory[J]. *Applied Mathematics and Mechanics*, 2019, **40**(12): 1321-1334. (in Chinese))
- [12] 曹源, 雷剑. 基于正弦剪切变形理论的功能梯度材料三明治微梁的静动态特性[J]. 复合材料学报, 2020, **37**(1): 223-235. (CAO Yuan, LEI Jian. Static and dynamic properties of functionally graded materials sandwich microbeams based sinusoidal shear deformation theory[J]. *Acta Materiae Compositae Sinica*, 2020, **37**(1): 223-235. (in Chinese))
- [13] THAI C H, FERREIRA A J M, TRAN T D, et al. A size-dependent quasi-3D isogeometric model for functionally graded graphene platelet-reinforced composite microplates based on the modified couple stress theory[J]. *Composite Structures*, 2020, **234**: 111695.
- [14] CARRERA E, BRISCHETTO S, CINEFRA M, et al. Effects of thickness stretching in functionally graded plates and shells[J]. *Composites Part B: Engineering*, 2011, **42**(2): 123-133.
- [15] NEVES A M A, FERREIRA A J M, CARRERA E, et al. A quasi-3D hyperbolic shear deformation theory for the static and free vibration analysis of functionally graded plates[J]. *Composite Structures*, 2012, **94**(5): 1814-1825.
- [16] LEE W H, HAN S C, PARK W T. A refined higher order shear and normal deformation theory for E-, P-, and S-FGM plates on Pasternak elastic foundation[J]. *Composite Structures*, 2015, **122**: 330-342.
- [17] ZHANG B, LI H, KONG L, et al. Size-dependent vibration and stability of moderately thick functionally graded micro-plates using a differential quadrature-based geometric mapping scheme[J]. *Engineering Analysis With Boundary Elements*, 2019, **108**: 339-365.
- [18] ZHANG B, LI H, KONG L, et al. Coupling effects of surface energy, strain gradient, and inertia gradient on the vibration behavior of small-scale beams[J]. *International Journal of Mechanical Sciences*, 2020, **184**: 105834.
- [19] ZHANG B, LI H, KONG L, et al. Size-dependent static and dynamic analysis of Reddy-type micro-beams by strain gradient differential quadrature finite element method[J]. *Thin-Walled Structures*, 2020, **148**: 106496.
- [20] ZHANG B, LI H, LIU J, et al. Surface energy-enriched gradient elastic Kirchhoff plate model and a novel weak-form solution scheme[J]. *European Journal of Mechanics A: Solids*, 2020, **85**: 104118.
- [21] VO T P, THAI H T, NGUYEN T K, et al. A quasi-3D theory for vibration and buckling of functionally graded sandwich beams[J]. *Composite Structures*, 2015, **119**: 1-12.